ACS OMEGA

Open Access

http://pubs.acs.org/journal/acsodf

Article

Using Diglycolamide Extractants in an Imidazolium-Based Ionic Liquid for Rare Earth Element Extraction and Recovery

Shu-An Hsieh, Tamalika Ash, Theresa L. Windus, Dapeng Jing, Tanya Prozorov, and Jared L. Anderson*

Cite This: *ACS Omega* 2024, 9, 40134−40144

Read Online

ACCESS | Metrics & More | Article Recommendations | Supporting Information

ABSTRACT: Growing demands for rare earth elements (REEs) have prompted sustainability concerns worldwide. Given the need for sustainable extraction methods amidst REEs, ionic liquids (ILs) have been investigated as tunable extraction substitutes for conventional organic solvents, offering negligible volatility and diverse physical and chemical properties. Recent reports have shown that the introduction of extractants, like N,N,N′,N′-tetraoctyldiglycolamide (TODGA) or N,N-dioctyldiglycolamic acid (DODGAA), into ILs can provide high selectivity and affinity for REE capture. Precipitate formation has been observed in IL-extractant systems across several studies; however, the molecular interactions that drive this phenomenon have yet to be explored. This study investigates the coordination environment in the precipitate formed between [Yb^{3+}], DODGAA, and the 1-butyl-3-methylimidazolium hexafluorophosphate ([$BMIM^+$][PF_6^-]) IL. The composition of the precipitate was confirmed using several spectroscopic techniques and revealed an underlying hydrogen bonding interaction between the fluorine atom of [PF_6^-] anion and −OH of the Yb-DODGAA complex. Computational studies were also conducted to examine the coordination environment of the Yb-TODGA and Yb-DODGAA complexes. The binding affinity of the extractants toward [Yb^{3+}] is analyzed by calculating the associated binding energy values. The results clearly show a stronger binding affinity of the extractants toward [Yb^{3+}], supporting the observed high extraction efficiencies of DODGAA and TODGA.

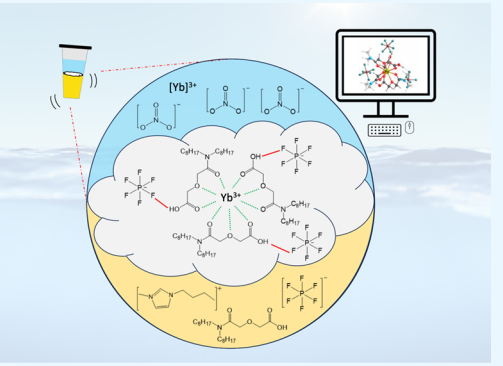

INTRODUCTION

Rare earth elements (REEs) are vitally important to the economic and national security of the United States and are of great significance for emerging technologies, defense, and clean energy applications. Ytterbium (Yb), one of the most widely used heavy REEs, possesses several unique properties that make it a crucial component in cutting-edge technologies such as sensors,[1] fiber optic lasers,[2] and magnets.[3] The importance of Yb in medical fields, including radiation therapy[4] and medical imaging,[5] highlights the need for sustainable practices to address issues related to the depletion of natural resources. Therefore, it is crucial to develop efficient recovery methods from sources such as mining residue[6] and discarded electronic waste.[7] Commonly used methods for recovering REEs involve chemical precipitation and solvent extraction with chemical precipitation being frequently applied for REE recovery due to its cost-effectiveness, simplicity, and ease of handling.[8] However, common oxalate precipitants are toxic and typically require energy-intensive conditions.[9] Solvent extraction, on the other hand, presents distinct advantages for REE recovery due to its scalability, adaptability to different metal-containing sources, and the potential for reducing energy consumption.[10,11] While organic solvents have been widely used for the recovery of REEs, drawbacks such as waste generation, toxicity, and high vaporization capability have prompted researchers to explore other classes of solvent systems for REE recovery.

Ionic liquids (ILs) possess highly tunable physical and chemical properties due to the various combinations of cations and anions.[12,13] Compared to conventional organic solvents, ILs are considered "greener and safer solvents" due to their low volatility and limited flammability.[14,15] Therefore, there is interest in substituting IL-based extraction systems for organic solvents to enable REE recovery.[16] There are no reports on the use of simple ILs, such as [$BMIM^+$][PF_6^-], for the effective and efficient extraction of [Yb^{3+}] ions. Therefore, the use of ILs tailored with specific functional groups to enhance the extraction efficiency for metals of interest has been explored.[17,18] Nevertheless, the production of functionalized ILs requires multiple synthetic steps, such as alkylation, neutralization, and metathesis, which is time-consuming and labor-intensive. The focus of IL-based REE extraction studies

Received: July 1, 2024
Revised: August 25, 2024
Accepted: September 2, 2024
Published: September 10, 2024

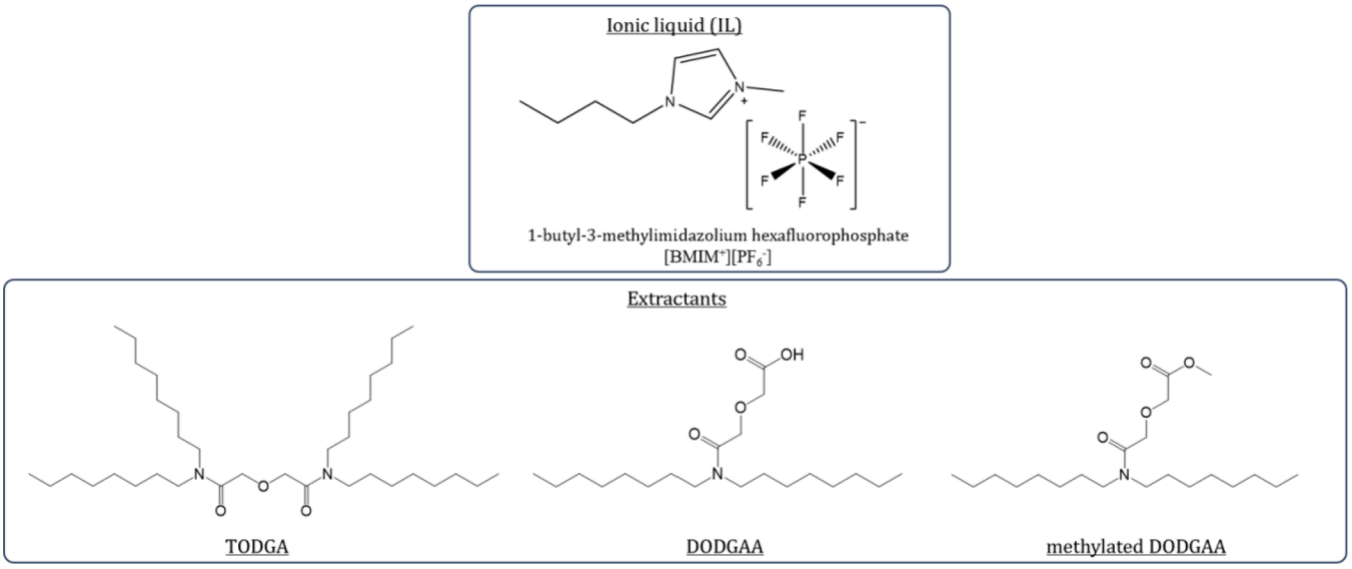

Figure 1. Chemical structures of the $[BMIM^+][PF_6^-]$ IL, and the diglycolamide-based extractants, TODGA, DODGAA, and methylated DODGAA, were evaluated in this study.

has predominantly centered on incorporating extractants into the IL system, which typically avoids appending functional groups to the IL. This approach aims to maintain high extraction efficiency and selectivity while avoiding complexities associated with the synthesis of functionalized ILs.[19] Diglycolamide-based (DGA) extractants, such as N,N,N′,N′-tetraoctyl diglycolamide (TODGA) and N,N-dioctyldiglycolamic acid (DODGAA), are among the most widely studied extractants due to their high selectivity in REE capture.[20,21] ILs containing the bis[(trifluoromethyl)sulfonyl] imide $[NTf_2^-]$ anion have been widely studied due to their hydrophobic nature in relation to the aqueous phase. Yang et al.[22] and Chen et al.[23] have both demonstrated the use of the $[BMIM^+][NTf_2^-]$ IL, coupled with the DGA-based extractant, resulting in higher selectivity for heavy REEs compared to a hydrocarbon-based organic solvent system. Hexafluorophosphate $[PF_6^-]$-based ILs are also known for their hydrophobic characteristics, yet few studies have investigated them in REE extractions largely due to the concern of hydrofluoric acid formation under certain conditions.[24] Nevertheless, the $[PF_6^-]$ anion still retains a number of noteworthy advantages, such as being cost-effective, having widespread availability, and generally producing lower viscosity ILs that aid in ease of handling and overall simple applicability.

Studies of IL-REE extraction have employed liquid−liquid extraction with two immiscible phases, along with spectroscopic and electrochemical techniques that probe the intricacies of these interactions to provide complete structural characterization.[19,25] Notably, the emergence of a precipitate as a third phase within the imidazolium-based IL extraction system has been widely observed and acknowledged, yet no study has thoroughly investigated the molecular binding environment surrounding the REE, extractant, and IL.[19,26] In addition, Zhou et al. showed the advantages of utilizing precipitation strategy as a recovery method using [trihexyl(tetradecyl)phosphonium]$_2$[4,4-isopropylidenebis(phenoxyacetate)]-functionalized IL.[27] Therefore, gaining an understanding of the composition and chemical coordination environment of the precipitate will provide stronger insights into the extraction mechanisms that underlie the REE capture with the extractant-IL system.

In this study, a detailed experimental and computational study was conducted to explore the chemical coordination environment of the precipitate formed in an extraction system containing ytterbium, DODGAA, and the $[BMIM^+][PF_6^-]$ IL. The amount of extracted REE was determined by liquid−liquid extraction and analyzed by inductively coupled plasma-optical emission spectroscopy (ICP-OES). A thorough molecular structural and composition analysis of the Yb-DODGAA precipitate was conducted by Fourier transform infrared spectroscopy (FTIR), scanning electron microscopy-energy dispersive spectrometry (SEM-EDS), X-ray photoelectron spectroscopy (XPS), and differential scanning calorimetry-thermogravimetric analysis (DSC-TGA). Moreover, the molecular binding environment was explored computationally using density functional theory (DFT) to examine the structural geometries, coordination environment, and binding energy of the associated complexes.

EXPERIMENTAL SECTION

Materials and reagents. The reagents 1-chlorobutane (≥99%), 1-methylimidazole (99%), potassium hexafluorophosphate, N,N,N,N-tetraoctyl diglycolamide (95%), dioctylamine (97%), thionyl chloride (99%), methanol (MeOH, HPLC grade), acetonitrile (ACN, HPLC grade), ethyl acetate (EA, ACS solvent grade), dichloromethane (DCM, ACS solvent grade), hydrochloric acid (HCl, 37%), and ytterbium nitrate pentahydrate (99.9%) were purchased from Sigma-Aldrich (St. Louis, MO, USA). Deionized nanopure water (18.2 MΩ·cm), obtained from a Millipore Milli-Q water purification system, was used to prepare all standard solutions. Diglycolic anhydride (>98%) was purchased from the Tokyo Chemical Industry (TCI, Chuo-ku, Tokyo, Japan). Nitric acid (99.99+ %), anhydrous methanol (99.9%), hexanes (certified ACS grade), polypropylene centrifuge tubes (1.5, 5, and 15 mL), 1 mL syringes with Luer-Lok tip, 5 mL norm-ject Luer-Lok tip, and 18G syringe needles were purchased from Thermo Fisher Scientific (Waltham, MA, USA). All procedures used to prepare ILs and extractants in this study are provided in the

https://doi.org/10.1021/acsomega.4c06091
ACS Omega 2024, 9, 40134−40144

Supporting Information (SI), and the chemical structures are shown in Figure 1.

Liquid−Liquid Extraction of [Yb^{3+}] Ions. A Fisherbrand analogue vortex mixer coupled with a foam insert set was used to perform agitation for all extractions. An Eppendorf 5920R benchtop centrifuge (Hamburg, Germany) was used to accelerate the process of separating the aqueous phase and the IL phase after agitation. A Bruker Neo-400 MHz nuclear magnetic resonance (NMR) spectrometer (Billerica, MA, USA) was used to characterize all of the synthesized compounds.

All extraction studies were carried out using ytterbium nitrate pentahydrate salt as the metal ion source. Nitric acid was selected as a pH control agent due to its strong dissociation and the simplicity it offers by minimizing the variety of anions present in the extraction system. An initial concentration of 100 ppm [Yb^{3+}] in 0.01 M nitric acid was used for all extraction studies, except for experiments that investigated the effect of nitric acid concentration. The added extractant in the system was premixed with the IL prior to the extraction to achieve a homogeneous system, ensuring consistent and effective interaction with [Yb^{3+}] in the aqueous phase. A 1:1 volume ratio of the aqueous and IL phases was mixed in a sealed polypropylene tube and vigorously shaken by vortex at 28 °C for 10 min to reach equilibrium. After the agitation was complete, the tube was centrifuged at 3000 rpm for 1 min to facilitate a clear, two-phase separation.

Inductively Coupled Plasma-Optical Emission Spectroscopy (ICP-OES). The metal ion concentration present in the aqueous phase was determined with an Agilent Technologies 5800 ICP-OES coupled to an SPS 4 autosampler (Santa Clara, CA, USA). For sample preparation, a 0.3 mL aliquot was withdrawn from the aqueous phase of the sample and pipetted into 2.7 mL of 2% (v/v) nitric acid solution in a 15 mL polypropylene tube. The mixture was vortexed for 30 s prior to ICP-OES analysis. A wavelength of 328.9 nm was selected for the measurement of [Yb^{3+}] from the sample. Standard solutions were first prepared at a [Yb^{3+}] concentration of 1000 ppm from $Yb(NO_3)_3{\cdot}5H_2O$ in 2% v/v HNO_3 solution. The calibration solutions were then diluted from the standard solution to concentrations of 0.005, 0.05, 0.1, 0.5, 1, 2, 4, 6, 8, and 10 ppm.

The metal ion concentration in the aqueous phase was measured using ICP-OES, and the extraction efficiency (%E) of [Yb^{3+}] in the IL was calculated from eq 1:

$$\text{Extraction efficiency (\% E)} = \frac{[M]_{IL,eq.}}{[M]_{aq.,ini.}} \times 100 = \frac{[M]_{aq.,ini.} - [M]_{aq.,eq.}}{[M]_{aq.,ini.}} \times 100 \quad (1)$$

where [M] represents the concentration of metal ion, aq. stands for the aqueous phase, IL represents the IL phase, ini. symbolized the initial state, and eq means the equilibrium state.

The distribution ratio (D) of [Yb^{3+}] in the two phases was calculated from eq 2:

$$\text{Distribution ratio} = [Yb(L)_3{}^{3+}]_{IL} / [Yb^{3+}]_{aq} \quad (2)$$

where L represents the extractants (TODGA or DODGAA).

Precipitate Recovery from DODGAA-[$BMIM^+$][PF_6^-] System. A solid precipitate was observed to form a third phase upon loading a high concentration (5×10^4 ppm) of [Yb^{3+}] in 1 mL of 0.01 M nitric acid solution. Liquid−liquid extraction was performed with 100 mM DODGAA dissolved in the [$BMIM^+$][PF_6^-] IL extraction phase. A 1:1 volume ratio of the aqueous and DODGAA-IL phases was mixed in a 5 mL sealed polypropylene tube and vigorously shaken by vortex at 28 °C for 10 min. After agitation, the solid white precipitate was recovered by vacuum filtration and extensively washed with 90 °C DI water to ensure that no IL residue was present. The precipitate was then placed in a vacuum oven at 28 °C for 24 h prior to all analyses.

Attenuated Total Reflectance-Fourier-Transform Infrared Spectroscopy (ATR-FTIR). All IR spectra were collected with a Bruker tensor 37 FTIR instrument equipped with a diamond ATR attachment. Background and sample measurements were acquired by averaging 32 scans with a spectral range from 400 to 4000 cm^{-1} and a spectral resolution of 1 cm^{-1} using the transmittance mode. All solid and liquid samples were placed directly on the diamond ATR for analysis without any sample preparation. OPUS 7.2 software from Bruker was used for the data acquisition and analysis.

Differential Scanning Calorimetry-Thermogravimetric Analysis (DSC-TGA). A STA449F1 DSC-TGA instrument from Netzsch (Selb, Germany) was used to conduct the analysis. All experiments were carried out under a nitrogen atmosphere using a temperature program from 40 to 1000 °C with a heating rate of 10 °C min^{-1}. Each sample was placed in a capped Al_2O_3 crucible with a sample mass of approximately 5−10 mg. Proteus software was used for the data acquisition and processing.

Scanning Electron Microscope-Energy Dispersive X-ray Spectroscopy Analysis (SEM-EDS). A Quanta-FEG 250 field-emission SEM-EDS instrument from FEI Company (Hillsboro, OR, USA) was used to observe the morphology of the precipitate obtained from the REE using the [$BMIM^+$][PF_6^-] IL. SEM was carried out under high vacuum mode at a working voltage of 10 kV beam. One backscattered electron image is presented in Figure S9. Qualitative elemental analysis was conducted using EDS to collect evidence of the [Yb^{3+}] existing in the white precipitate as well as tentative identification of species following thermal analysis. Sample preparation for SEM-EDS analysis on the precipitate involved sprinkling the dried white precipitate onto double-sided carbon tape mounted on a carbon substrate. A layer of iridium (2 nm thickness) was coated on the sample using a Q150T sputter coater, from Quorum Technologies Inc. (East Sussex., United Kingdom), to increase the conductivity of the sample.

X-ray Photoelectron Spectroscopy (XPS). XPS analyses were carried out on a Kratos Amicus XPS system using an Al Kα lab X-ray source. The loose powder sample was spread onto double-sided adhesive tape. A wide scan was first collected with an energy step of 1 eV, followed by high-resolution scans with an energy step of 0.1 eV for the regions of interest. Peak fitting was conducted with CasaXPS software (version 2.3.19).

Density Functional Theory (DFT) Calculations. The electronic structure calculations were performed using the NWChem 7.0.2[28] quantum chemistry program. The geometries of all complexes were optimized by employing the B3LYP exchange-correlation functional.[29,30] All gas and solvent phase geometry optimizations were performed by using the

https://doi.org/10.1021/acsomega.4c06091
ACS Omega 2024, 9, 40134−40144

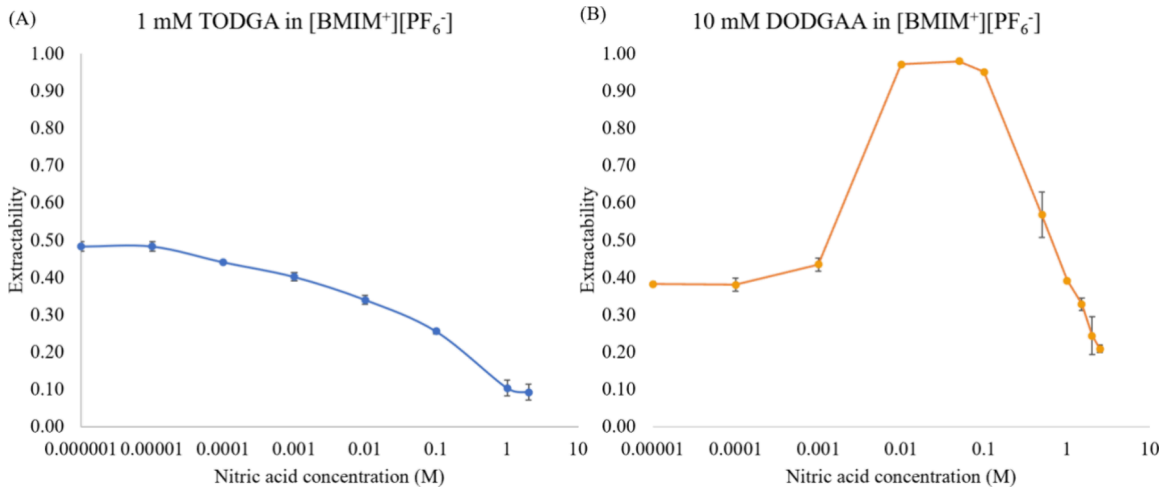

Figure 2. Examining the effect of nitric acid concentration on the extraction efficiency of $[Yb^{3+}]$ using TODGA and DODGAA extractants dissolved in the $[BMIM^+][PF_6^-]$ IL. Blue and orange lines represent (A) 1 mM of TODGA and (B) 10 mM of DODGAA, respectively, dissolved in IL as the extractant. Extraction conditions: ytterbium ion concentration: 100 ppm; extraction time: 10 min; extraction temperature: 28 °C; vortex: 2600 rpm; extraction volume ratio: 1:1 (aqueous phase to organic phase). Triplicate measurements were performed for each condition.

def2-svp[31,32] basis set for the main group elements and Stuttgart RSC Segmented basis set and ECP with 28 core electrons[33,34] for Yb, which reduces the calculation expense and accounts for scalar relativistic effects. The van der Waals interactions were accounted for through empirical long-range contributions employing Grimme's dispersion (D3).[35] The solvent phase calculations were performed using the implicit Solvation Model Based on Density (SMD) continuum solvation model[36] for water and IL. Here, for water, the default parameters implemented in NWChem have been used, and the IL parameters were taken from the work of Anderson et al.[37] and Wakai et al.[38]

The binding energy (BE) of the complexes was calculated using the following equations

$$[Yb(H_2O)_9^{3+}]_{(aq)} + 3[L]_{(IL)} + 3[PF_6^-]_{(IL)} \rightarrow [Yb(L)_3(PF_6)_3]_{(IL)} + 9[H_2O]_{(aq)} \quad (3)$$

$$BE = E([Yb(L)_3(PF_6)_3]_{(IL)}) + 9^*E([H_2O]_{(aq)}) - E([Yb(H_2O)_9^{3+}]_{(aq)}) - 3^*E([L]_{(IL)}) - 3^*E([PF_6^-]_{(IL)}) \quad (4)$$

where L = TODGA/DODGAA, (aq) and (IL) indicate the continuum solvation model around the species, and E() means the energy of the moiety within the parentheses.

To carry out the study, we considered the methyl derivative of DODGAA and TODGA to reduce the computational cost. In the SI, the DFT energy values for each complex are provided. In addition, we have performed Natural Population Analysis (NPA) of free DODGAA and TODGA ligands using the JANPA software package.[39,40]

RESULTS AND DISCUSSION

Optimization of Extraction Time and Nitric Acid Concentration. Prior to investigating the extraction mechanism of $[Yb^{3+}]$ with the $[BMIM^+][PF_6^-]$ IL, we evaluated the extraction time and the concentration of nitric acid in the extraction system. Figure S10 shows the relationship between the extraction efficiency of $[Yb^{3+}]$ with the $[BMIM^+][PF_6^-]$ IL as a function of the extraction time for two distinct systems. The blue and orange lines in the figure represent TODGA (1 mM) and DODGAA (10 mM) dissolved in the $[BMIM^+][PF_6^-]$ IL phase, respectively. Notably, a lower concentration of TODGA was employed due to the lack of a discernible trend in extraction efficiency when a concentration of 10 mM TODGA was used. Both systems contained an initial $[Yb^{3+}]$ concentration of 100 mM. A series of extraction times ranging from 0 to 40 min were applied, and an optimal extraction time of 10 min was selected to ensure both systems attained equilibrium and was used for all subsequent studies.

To evaluate the extraction efficiency of $[Yb^{3+}]$ using TODGA/DODGAA in the $[BMIM^+][PF_6^-]$ IL, the effect of the nitric acid concentration in the extraction systems was investigated. Figure 2 shows that in the TODGA-$[BMIM^+][PF_6^-]$ system, lower nitric acid concentration levels led to an increase in $[Yb^{3+}]$ extraction efficiency, reaching a plateau at lower nitric acid concentration (10^{-5} M). For the DODGAA-$[BMIM^+][PF_6^-]$ system, a similar decreasing trend was observed when the nitric acid concentration varied from 10^{-2} to 1.4 M. However, a more than 50% drop in extraction efficiency was observed when the nitric acid concentration decreased from 10^{-2} to 10^{-5} M. This reduction can be attributed to the pK_a of DODGAA, which is approximately 3.54. As the concentration of nitric acid decreases, the partial deprotonated DODGAA impairs its ability to effectively coordinate and extract $[Yb^{3+}]$, resulting in the diminished extraction efficiency.[41] These results appear to indicate that DODGAA behaves as a neutral tridentate extractant, much like TODGA.[19] Based on these results, subsequent extraction studies employed a nitric acid concentration of 10^{-5} and 10^{-2} M for the TODGA and DODGAA systems, respectively.

Extraction Mechanism of $[Yb^{3+}]$ using DODGAA and TODGA Extractants. Several extractants have been investigated to facilitate a cation-exchange extraction mechanism in the IL system, in contrast to an ion-pair extraction mechanism that predominates in the organic solvent extraction system.[42,43] For $[Yb^{3+}]$ extraction using TODGA/DODGAA dissolved in ILs, a noteworthy trend was observed. The extraction efficiency of $[Yb^{3+}]$ was found to decrease when higher amounts of nitric acid were added to the extraction system. This observation

https://doi.org/10.1021/acsomega.4c06091
ACS Omega 2024, 9, 40134−40144

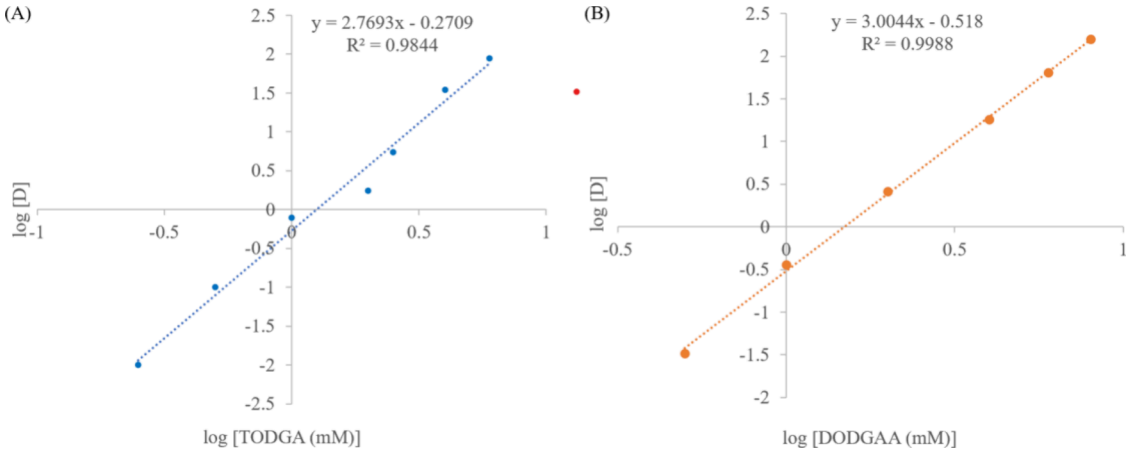

Figure 3. Slope analysis for ytterbium extraction as a function of (A) TODGA and (B) DODGAA concentrations in the $[BMIM^+][PF_6^-]$ IL. Extraction conditions include: extraction time: 10 min; extraction temperature: 28 °C; vortex rate: 2600 rpm; $[HNO_3] = 10^{-5}$ M for the TODGAA system, whereas $[HNO_3] = 10^{-2}$ M while using DODGAA as an extractant. A volume ratio of 1:1 (aqueous phase to organic phase) was applied. Triplicate measurements were performed for each condition.

Table 1. Investigation into the Occurrence of Precipitation Formation Was Performed by Varying the Concentration of Extractant (TODGA or DODGAA) in the $[BMIM^+][PF_6^-]$ IL Extraction System[a,b,c,d,e]

	ionic liquid	$[BMIM^+][PF_6^-]$									
extraction conditions	time (min)	10 min									
	vortex rate (rpm)	2600									
	temperature (°C)	28									
	phase ratio (V_{aq}/V_{IL})	1:1									
	type of acid	nitric acid									
	type of extractant	TODGA			DODGAA						
	extractant concentration (mM)	1	10	100	1		10		100		
	acid concentration (M)	10^{-5}			10^{-2}						
	ytterbium(III) concentration (ppm)	100/Sat.			100	Sat.	100	Sat.	100	Sat.	
precipitate formation		N			N	Y	Y	Y	Y	Y	

[a]Extraction conditions including extraction time, vortex rate, temperature, phase ratio between the aqueous phase and the IL phase, type of acid, type of extractant, extractant concentration, acid concentration, and the initial concentration ytterbium ion are provided. [b]"V_{aq}" represents volume of the aqueous phase; "V_{IL}" represents volume of the IL phase. [c]"Sat." represents using 5×10^4 ppm of ytterbium(III) to create a high concentration of ytterbium ion present in the system. [d]Precipitate refers to the remaining solid after treated with vacuum overnight. [e]"N" represents that no precipitate formation was found after agitation; "Y" represents a precipitate formation.

suggests that nitrate ions do not undergo coextraction into the IL phase[44] and do not participate as counteranions during the extraction of $[Yb^{3+}]$. This can be further supported by spectroscopic data obtained in subsequent studies. Therefore, it can be inferred that $[PF_6^-]$ remains in the IL phase, while $[Yb^{3+}]$ is extracted within the IL-extractant phase. To maintain charge balance, the $[BMIM^+]$ cation of the IL can be released into the aqueous phase.[23] To verify this, varying amounts of the $[BMIM^+][Cl^-]$ IL were introduced into the aqueous phase. As shown in Figure S11, both the TODGA and DODGAA systems produced lower extraction efficiency of $[Yb^{3+}]$ with an increasing concentration of $[BMIM^+]$ in the aqueous phase, supporting the notion that both extractants exhibit a cation-exchange mechanism that involves the release of $[BMIM^+]$ into the aqueous phase and extraction of $[Yb^{3+}]$ into the IL phase.

The extraction mechanism of $[Yb^{3+}]$ using either TODGA or DODGAA was subsequently examined through slope analysis to elucidate the stoichiometric relationship between the metal ion and the extractants.[45] By examination of the slope between $[Yb^{3+}]$ and the extractant, the slope analysis can provide information about the number of TODGA or DODGAA molecules involved in complexation with $[Yb^{3+}]$. Based on the slope analysis, the extraction equilibrium equation of $[Yb^{3+}]$ using these two extractants was determined according to eq 5:

$$[Yb^{3+}]_{aq.} + 3L_{IL} + 3[BMIM^+]_{IL} \leftrightarrow Yb(L)_3^{3+}{}_{IL} + 3[BMIM^+]_{aq} \quad (5)$$

where L represents the extractant (TODGAA or DODGAA), aq. stands for the aqueous phase, and IL represents the IL phase. The extraction equilibrium constant (K_{eq}) for the migration of the trivalent metal ions $[Yb^{3+}]$ through a cation-exchange process is formulated by eq 6:

$$K_{eq} = [Yb(L)_3^{3+}]_{IL}[BMIM^+]_{aq.}^3/[Yb^{3+}]_{aq.}[L]_{IL}^3 [BMIM^+]_{IL}^3 \quad (6)$$

The equation can also be rewritten by substituting the distribution ratio $D = [Yb(L)_3^{3+}]_{IL}/[Yb^{3+}]_{aq}$, as shown:

$$K_{eq} = D[BMIM^+]_{aq.}^3/[L]_{IL}[BMIM^+]_{IL}^3 \quad (7)$$

This equation can also be converted into its logarithmic form, as shown in eq 8:

https://doi.org/10.1021/acsomega.4c06091
ACS Omega 2024, 9, 40134−40144

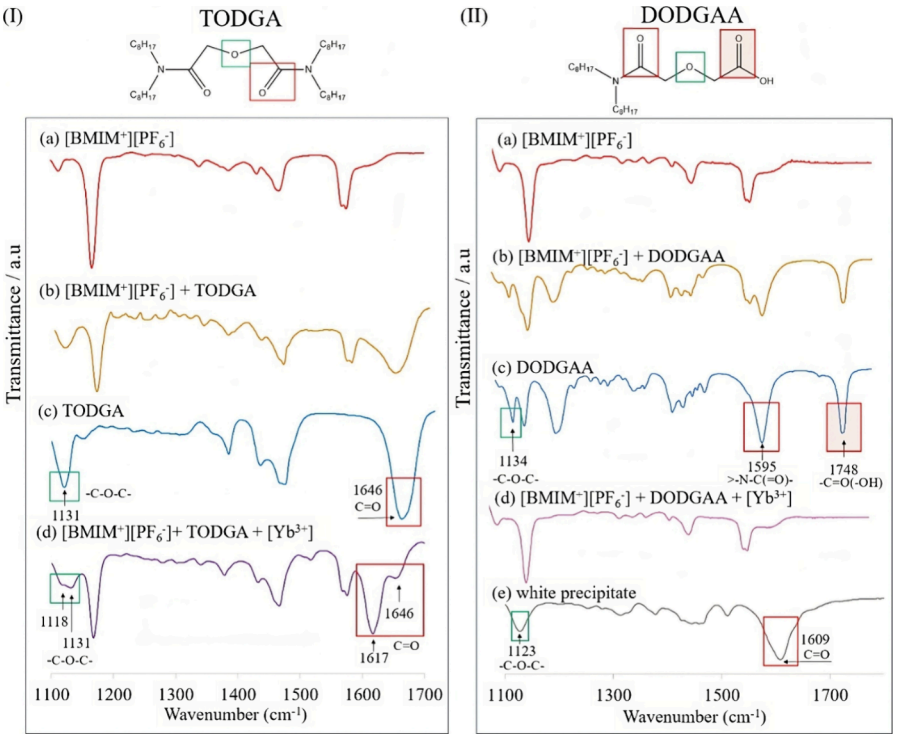

Figure 4. Attenuated total reflectance-Fourier transform infrared (ATR-FTIR) analysis of the TODGA and DODGAA specimens. Panel (I) shows spectra for (a) $[BMIM^+][PF_6^-]$ IL, (b) $[BMIM^+][PF_6^-]$ + TODGA, (c) TODGA, and (d) $[BMIM^+][PF_6^-]$ + TODGA + $[Yb^{3+}]$. Panel (II) shows spectra of (a) $[BMIM^+][PF_6^-]$ IL, (b) $[BMIM^+][PF_6^-]$ + DODGAA, (c) DODGAA, (d) $[BMIM^+][PF_6^-]$ + TODGA, and (e) white precipitate obtained from the extraction using 100 mM of DODGAA in $[BMIM^+][PF_6^-]$ with 5×10^4 ppm of $[Yb^{3+}]$.

$$\text{Log } D = \log[L]_{IL} + 3\log[BMIM^+]_{IL} + \log K_{eq} - 3\log[BMIM^+]_{aq} \quad (8)$$

For example, Figure 3 shows the logarithmic plots of the distribution ratio of $[Yb^{3+}]$ versus the concentration of (A) TODGA and (B) DODGAA. Linear regression of both plots provides slopes of approximately 3, suggesting that three molecules of the extractants (TODGA or DODGAA) are involved in forming the ytterbium complex. Simultaneously, three $[BMIM^+]$ ions from the IL phase are presumably released into the aqueous phase, while one $[Yb^{3+}]$ ion is extracted.

Effect of Initial $[Yb^{3+}]$ Concentration and TODGA/DODGAA on Precipitate Formation. Extraction of $[Yb^{3+}]$ using 10 mM DODGAA with 50,000 ppm of $[Yb^{3+}]$ resulted in the formation of a white solid precipitate (Figure S12B), which was not observed in the TODGA system (Figure S12A). Therefore, an investigation was undertaken to explore the effect of the initial $[Yb^{3+}]$ concentration and variation in the TODGA/DODGAA concentration in the system on the formation of the precipitate. Irrespective of the concentrations of TODGA and $[Yb^{3+}]$ present in the extraction system, no precipitate was observed, as shown in Table 1. In contrast, the extraction system employing DODGAA as an extractant revealed the emergence of a precipitate when the initial $[Yb^{3+}]$ concentration was increased. When the DODGAA concentration exceeded 10 mM, the precipitate was observed in both conditions, whether either 100 or 50,000 ppm of $[Yb^{3+}]$ was introduced into the initial aqueous phase. The formed precipitate was collected for further spectroscopic analysis to unravel its structural and compositional characteristics.

Investigating Molecular Interactions within DODGAA-$[BMIM^+][PF_6^-]$ Precipitate. *Molecular Interaction Study Using Attenuated Total Reflectance-Fourier-Transform Infrared Spectroscopy (ATR-FTIR).* To further study the composition of the precipitate formed during the extraction process, ATR-FTIR spectra were used to identify their functional groups and investigate possible molecular interactions.[27] TODGA comprises two amide carbonyl moieties and an ether group, as shown in Figure 4I. Characteristic peaks in the FTIR spectrum for TODGA are highlighted by the asymmetric (−C−O−C−) stretching of the ether group, observed at 1131 cm^{-1}, and carbonyl (>N−C═O) stretching of the amide group at 1646 cm^{-1}. Figure 4I-d was obtained by loading $[Yb^{3+}]$ into a mixture containing 0.15 M TODGA in the $[BMIM^+][PF_6^-]$ IL for extraction. A shoulder peak was observed at 1118 cm^{-1}, which correlates to regions of the −C−O−C− stretching, while the C═O stretch occurred at a significant shift from 1646 to 1617 cm^{-1} in the spectrum.[46] These results suggest that the two carbonyl groups and the ether group in TODGA actively participate in coordination during the extraction of $[Yb^{3+}]$.

FTIR spectra of the DODGAA extraction system are shown in Figure 4II. Similarly, DODGAA exhibits distinctive peaks in its IR spectra, including an ether group (−C−O−C−) observed at a wavenumber of 1134 cm^{-1}, a carbonyl moiety (>−N−C(═O)−) at 1595 cm^{-1}, and a carboxylic acid moiety (−C═O(−OH)) at 1748 cm^{-1}.[47] The extraction system comprising 100 mM DODGAA in $[BMIM^+][PF_6^-]$ with 5×10^4 ppm of $[Yb^{3+}]$ led to a notable appearance of a white precipitate. The precipitate and the IL phase were subsequently collected and subjected to separate IR analysis. Figure 4II-d shows FTIR spectra of the IL after the extraction,

https://doi.org/10.1021/acsomega.4c06091
ACS Omega 2024, 9, 40134−40144

revealing the absence of the two characteristic peaks (−C−O−C stretch and −C═O stretch) for DODGAA. Notably, the spectrum closely matched that of the [$BMIM^+$][PF_6^-] IL, suggesting that the majority of the DODGAA molecules participated in the extraction process since the resulting DODGAA-metal complex did not dissolve in the IL phase. The recovered white precipitate was then analyzed and revealed characteristic peaks similar to those of DODGAA. Specifically, peaks representing the −C═O stretch on DODGAA were shifted to 1609 cm^{-1}, and the −C−O−C stretch appeared at ∼1123 cm^{-1}. Additionally, the characteristic absorption peak of nitrate ranges from 1500 to 1200 cm^{-1}, which were not observed in the ATR-FTIR spectrum.[48] However, due to the ambiguity within the peak-overlapping region, interactions between the functional groups were unclear. Therefore, additional techniques were employed to investigate the chemical environment within the [Yb^{3+}]-DODGAA complex.

Assessing Thermal Stability of the System Using Differential Scanning Calorimetry-Thermogravimetric Analysis (DSC-TGA). DSC-TGA was employed to evaluate the thermal properties of the precipitate, DODGAA, and the [$BMIM^+$]-[PF_6^-] IL. The DSC-TGA curves, shown in Figure S13, revealed that the DODGAA extractant began to decompose at a temperature above 150 °C, whereas the white precipitate exhibited slightly higher thermal stability with decomposition at 240 °C. Additionally, the [$BMIM^+$][PF_6^-] IL exhibits nearly complete mass loss by 500 °C. After reaching 400 °C, the remaining mass from the DODGAA specimen was around 10−15%, while the white precipitate retained approximately 25% of its initial mass. This result strongly suggests the presence of metal ions in the precipitate due to the high decomposition temperature of the [Yb^{3+}] complex compared to that of DODGAA. Consequently, a higher residual mass was observed after exposing the precipitate to elevated temperatures.

Since the white precipitate was observed to form between the IL and aqueous layers, its recovery required a washing step for subsequent analysis. Various organic solvents, including acetone, dichloromethane, ethyl acetate, acetonitrile, methanol, ethanol, and ether, were tested to remove the IL residue from the precipitate. However, it was found that all examined organic solvents possess the capability of dissolving both the precipitate and the IL. Nevertheless, it was discovered that water at 90 °C served as an effective washing solution for removing the IL, while also preserving the precipitate. The DSC curve in Figure S13 showed an endothermic peak between 350 and 500 °C for the IL, while it was not observed on the DSC curve for the white precipitate. Therefore, it can be concluded that the IL was sufficiently removed from the precipitate by washing with water at 90 °C.

Analyzing Chemical Composition of Precipitate Using Scanning Electron Microscopy-Energy Dispersive X-ray Spectroscopy (SEM-EDS). SEM-EDS is a powerful technique that is used for surface imaging and provides information regarding the elemental composition of materials.[49] In Figure S9, SEM images show the morphology of the white precipitate. Despite various morphologies being observed within the sample, the EDS spectra reveal negligible differences in the composition of the chosen regions. The diagram also reveals that the specimen primarily consists of carbon (C), oxygen (O), nitrogen (N), ytterbium (Yb), phosphorus (P), and fluorine (F) and that this composition is consistent with the TGA findings, providing additional confirmation of [Yb^{3+}] recovery from the precipitate. Moreover, the absence of the nitrate peak (∼1346 cm^{-1})[50] from the FTIR spectrum (Figure 4) suggests that nitrate ions are unlikely counteranions in the complex. This observation is consistent with findings from a prior experiment involving the effect of varying concentrations of nitric acid in the extraction system and affirms that nitrate is not coextracted into the IL phase during the extraction of [Yb^{3+}]. As a result, it can be deduced that the [PF_6^-] anion is a prevailing component contributing to the formation of the white precipitate. Consequently, the precipitation mechanism can be written as follows in eq 9:

$$[Yb^{3+}]_{aq.} + 3[NO_3^-]_{aq.} + 3DODGAA_{IL} + 3[BMIM^+]_{IL} + 3[PF_6^-]_{IL} \rightarrow [Yb(DODGAA)_3^{3+}][PF_6^-]_3 \downarrow + 3[NO_3^-]_{aq.} + 3[BMIM^+]_{aq} \quad (9)$$

X-ray Photoelectron Spectroscopy (XPS) Analysis for Neat DODGAA and DODGAA-[$BMIM^+$][PF_6^-] Complex. To gain additional insights into the molecular-level interactions within the complex, XPS was employed. This technique offers information regarding the elemental composition and chemical states of the constituent elements present within a material.[51] Figure S14B shows components associated with the −C═O− moiety at 288 eV and C−C and C−H moieties at 284.8 eV from the neat DODGAA. An increased fraction of oxidized carbon was found in the precipitate. Another noteworthy change observed is that from the nitrogen region. Figure S14C shows a single symmetrical peak at 399.9 eV for neat DODGAA, while two different chemical environments of nitrogen atoms (399.7 and 401.4 eV) were observed for the precipitate. This change signifies that one or more nitrogen atoms in the metal complex serve as electron donors, and the three coordinated DODGAA molecules possess different coordination environments with [Yb^{3+}]. It was shown in a study by Shimojo et al.[52] that tautomerism can be observed in the DODGAA molecule wherein the C−N bond displays partial double-bond character when binding with the tertiary amide group, leading to lower basicity of the amide nitrogen atom (Figure S15). On the other hand, the amide oxygen atom exhibits an increased tendency to donate electron pairs, making it a more effective functional group for the formation of metal-coordinated complexes. Moreover, the absence of the nitrate ions in the complex was affirmed due to the lacking -NO_3 peak (∼407.2 ± 0.6 eV), which, again, aligns with the aforementioned argument that nitrate is not present as a counteranion in the precipitate.[53] In addition, fluorine atoms in the [PF_6^-] anion exhibit two different binding environments in the precipitate, measured at 686.0 and 688.2 eV, after peak deconvolution. The higher binding energy (688.2 eV) can be attributed to the F---H−O interaction, and the lower binding energy peak (686.0 eV) can be attributed to all other fluorine atoms in the [PF_6^-] anion. This observation suggests that a potential interaction occurs between the metal complex of the cation and the [PF_6^-] anion.

Extraction of [Yb^{3+}] with a Methylated Analogue of the DODGAA Molecule. To further investigate interactions related to the fluorine atoms of the [PF_6^-] anion in the precipitate, an experimental approach was conducted by substituting the chemical structure of DODGAA, particularly targeting the hydroxyl (−OH) moiety, which is likely to be involved in these interactions. TODGA contains four octyl

https://doi.org/10.1021/acsomega.4c06091
ACS Omega 2024, 9, 40134−40144

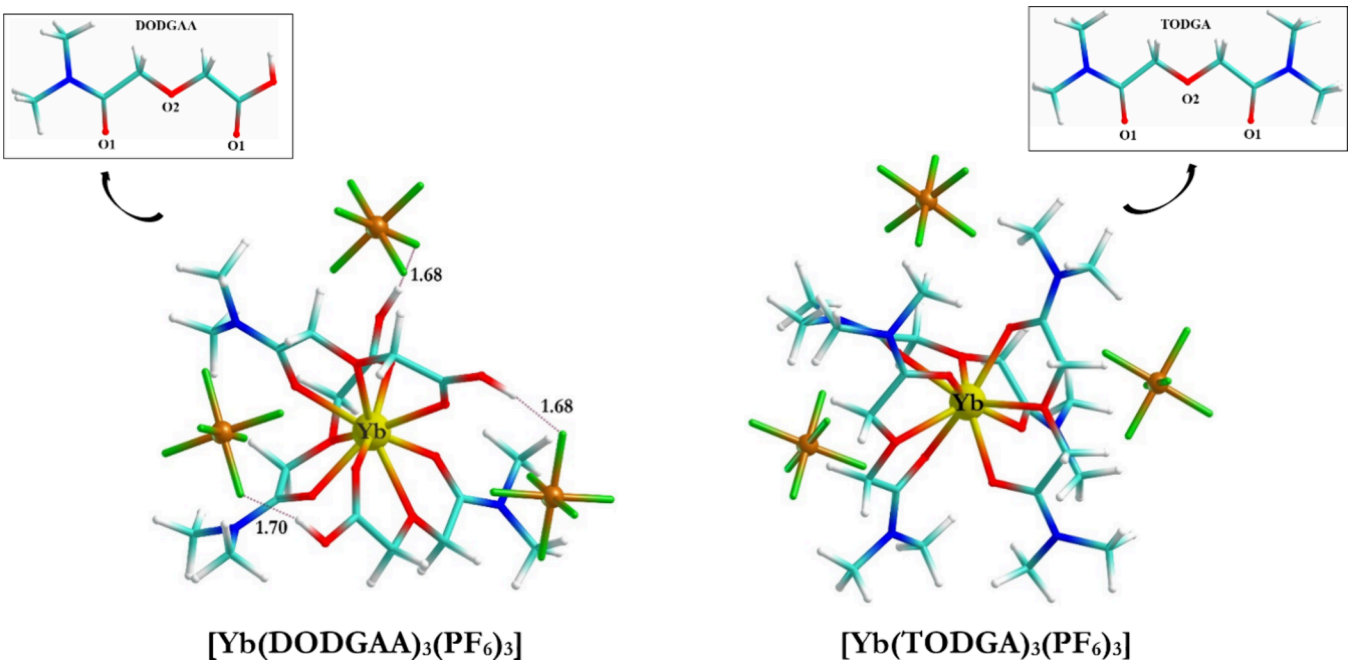

Figure 5. Optimized geometries of $[Yb(DODGAA)_3(PF_6)_3]$ and $[Yb(TODGA)_3(PF_6)_3]$ complexes in the RTIL continuum solvation model. Bond lengths are given in Å. Yellow = ytterbium, red = oxygen, blue = nitrogen, turquoise = carbon, white = hydrogen, orange = phosphorus, green = fluorine.

groups attached to a central glycolamide unit, whereas DODGAA possesses two octyl groups on one end of the molecule and a carboxylic acid moiety on the other. From Table 1, no precipitate was observed in the TODGA extraction system regardless of the concentration of TODGA or $[Yb^{3+}]$ involved in the extraction system. An assumption was made that the −OH group may be involved in hydrogen bonding interactions with one of the fluorine atoms of the $[PF_6^-]$ anion, contributing to the occurrence of the precipitate in the DODGAA system. Therefore, a methylated DODGAA molecule was synthesized and used as an extractant.[54] Methylated DODGAA, as shown in Figure 1, involved substituting the hydroxyl group (−OH) with a methoxy group ($-OCH_3$), thereby eliminating the potential for hydrogen bonding interactions between the −OH moiety and the fluorine atom. As a result, Figure S16B shows that no precipitate was observed even upon adding 100 mM of methylated DODGAA in the $[BMIM^+][PF_6^-]$ IL loaded with 5×10^4 ppm of $[Yb^{3+}]$.

Density Functional Theory (DFT) Analysis. To gain a comprehensive understanding of the intricate geometries arising from the interaction between $[Yb^{3+}]$ and DGA ligands [L], DFT analysis was performed. Following the experimental findings, a single $[Yb^{3+}]$ cation undergoes complexation with three DGA ligands, leading to the formation of the $[Yb(L)_3]^{3+}$ complex. The absence of $[NO_3^-]$ was confirmed from FTIR and SEM-EDS analyses, suggesting the likely presence of $[PF_6^-]$ as the counteranion of the $[Yb(L)_3]^{3+}$ complex for charge neutralization. Following this hypothesis for the theoretical modeling, three molecules of $[PF_6^-]$ were included to neutralize the charge of the $[Yb(L)_3]^{3+}$ complex, resulting in the final complex $[Yb(L)_3(PF_6)_3]$.

As illustrated in Figure 5, the geometry analysis of the $[Yb(DODGAA)_3(PF_6)_3]$ complex reveals that it is a 9-coordinated complex, where the DODGAA ligand coordinates to $[Yb^{3+}]$ as a tridentate ligand via two −C═O (we will label this oxygen as O1) and $-CH_2-O-CH_2-$ (labeling this oxygen as O2). Notably, the O1−Yb distances exhibit slight variations, with shorter distances (2.27−2.29 Å) observed when adjacent to $-NMe_2$ compared with the O1−Yb distances (2.30−2.37 Å) adjacent to −OH (Table S1). The NPA charge (Table S2) calculated for the free DODGAA ligand shows that the NPA charge on the $-NMe_2$ adjacent to O1 is −0.606, whereas for the −OH adjacent to O1, the value is −0.546, implying a greater electron-donating tendency of the former O1 than that of the later O1. This result corresponds well with the XPS finding, indicating that amide oxygen atoms have a greater tendency to donate electrons, resulting in stronger binding. The O2−Yb distances are calculated to be longer (2.43−2.52 Å) than O1−Yb. The NPA charge on the O2 center (−0.553) is lower than $-NMe_2$ adjacent to O1 but almost equal to the −OH adjacent to O1. The $[PF_6^-]$ anions are in the second coordination sphere and interact with $[Yb(DODGAA)_3]^{3+}$ through their fluoride ends via the formation of H···F hydrogen bonds (1.68−1.70 Å) with the −OH moiety of DODGAA. Therefore, the electronic environment surrounding the hydrogen-bonded fluorine atoms differs from that of non-hydrogen-bonded fluorine atoms, as clearly demonstrated by the XPS study. Moreover, the actual persistence of the hydrogen bonding interaction between $[Yb(DODGAA)_3]^{3+}$ and $[PF_6^-]$, which may account for precipitate formation from experimental observation, is further validated through DFT analysis. In the case of the TODGA ligand, a similar 9-coordinated $[Yb(TODGA)_3(PF_6)_3]$ complex is formed, where the O1−Yb distances range between 2.28 and 2.33 Å and O2−Yb distances between 2.42 and 2.51 Å. The NPA charge on the O1 centers is −0.607, which is greater than that for the O2 center of −0.551, suggesting a greater electron-donating tendency of amide oxygens than the ether oxygen. Unlike the case for the DODGAA complex, there is no possibility of hydrogen bond formation between $[Yb(TODGA)_3^{3+}]$ and $[PF_6^-]$. Analyzing the binding energy

https://doi.org/10.1021/acsomega.4c06091
ACS Omega 2024, 9, 40134−40144

values in the RTIL continuum solvation model tabulated in Table 2, calculated following eq 4, reveals a total binding energy (BE) of −122.9 kcal/mol for the [Yb(DODGAA)$_3$(PF$_6$)$_3$] complex and −129.2 kcal/mol for the [Yb(TODGA)$_3$(PF$_6$)$_3$] complex. The slightly higher BE for the TODGA complex compared to the DODGAA complex can also be explained by the higher electron-donating tendency of the directly coordinated O1 centers for TODGA to [Yb^{3+}] than that of DODGAA. Therefore, it is evident that irrespective of the choice of the extracting ligand, both DODGAA and TODGA show high binding affinity toward [Yb^{3+}], indicating their effectiveness as extraction agents.

Table 2. Binding Energy (BE) Values of [Yb(L)$_3$(PF$_6$)$_3$] (L = TODGA/DODGAA) Complexes in the RTIL Continuum Solvation Model[a]

[Yb(L)$_3$(PF$_6$)$_3$] complexes	BE
[Yb(TODGA)$_3$(PF$_6$)$_3$]	−129.2
[Yb(DODGAA)$_3$(PF$_6$)$_3$]	−122.9

[a]The values are given in kcal/mol.

CONCLUSIONS

This study investigates the molecular interactions among [Yb^{3+}], DODGAA, and the [BMIM$^+$][PF$_6^-$] IL, providing insights into the extraction mechanism that leads to precipitate formation. The Yb-DODGAA complex, confirmed via ATR-FTIR, SEM-EDS, and DSC-TGA techniques, involves the [PF$_6^-$] anion as the counteranion, as indicated by the absence of [NO$_3^-$]. Hydrogen bonding between the fluorine atom of [PF$_6^-$] and the −OH moiety of DODGAA, critical for precipitate formation, was confirmed through experimental methylated DODGAA studies and DFT analysis. This interaction is absent in the [Yb(TODGA)$_3$(PF$_6$)$_3$] complex, which does not form precipitates despite the similar binding affinities for [Yb^{3+}]. Precipitation offers a highly efficient method for REE recovery, allowing single-step solid−liquid separation and improving recovery efficiency and sustainability. Future investigations into the combustion of the Yb-DODGAA complex will lead to refining the recovery process of [Yb^{3+}] as its oxide form, Yb$_2$O$_3$. Additionally, a comprehensive understanding of the stability of the precipitate under various pH levels is essential for optimizing industrial extraction processes due to the fact that lower pH typically favors precipitation by making the process more thermodynamically favorable, while excessive acidic conditions can disrupt the formation of the precipitate in the system. Insights from this study enhance the understanding of REE extraction mechanisms and suggest avenues for optimizing experimental conditions, exploring additional IL-extractant systems, and evaluating scalability for industrial applications.

ASSOCIATED CONTENT

Supporting Information

The Supporting Information is available free of charge at https://pubs.acs.org/doi/10.1021/acsomega.4c06091.

Synthesis procedures of ILs and extractants, ^{1}H NMR and ^{13}C NMR spectra, SEM-EDS spectra, optimization of extraction time for [Yb^{3+}] extraction efficiency, effect of [BMIM$^+$][Cl$^-$] on extraction efficiency, images of precipitate, DSC-TGA, XPS survey, tautomerism of DODGAA framework, details of RTIL parameters used for computational calculations, and xyz coordinates of the optimized complexes in RTIL continuum solvation model (PDF)

AUTHOR INFORMATION

Corresponding Author

Jared L. Anderson − *Ames National Laboratory, U.S. Department of Energy, Ames, Iowa 50011, United States; Department of Chemistry, Iowa State University, Ames, Iowa 50011, United States;* orcid.org/0000-0001-6915-8752; Phone: +1 515-294-8356; Email: andersoj@iastate.edu

Authors

Shu-An Hsieh − *Ames National Laboratory, U.S. Department of Energy, Ames, Iowa 50011, United States; Department of Chemistry, Iowa State University, Ames, Iowa 50011, United States*

Tamalika Ash − *Ames National Laboratory, U.S. Department of Energy, Ames, Iowa 50011, United States;* orcid.org/0000-0002-7736-7770

Theresa L. Windus − *Ames National Laboratory, U.S. Department of Energy, Ames, Iowa 50011, United States; Department of Chemistry, Iowa State University, Ames, Iowa 50011, United States;* orcid.org/0000-0001-6065-3167

Dapeng Jing − *The Materials Analysis Research Laboratory, Iowa State University, Ames, Iowa 50011, United States;* orcid.org/0000-0001-7600-7071

Tanya Prozorov − *Ames National Laboratory, U.S. Department of Energy, Ames, Iowa 50011, United States;* orcid.org/0000-0001-7792-4103

Complete contact information is available at: https://pubs.acs.org/10.1021/acsomega.4c06091

Notes

The authors declare no competing financial interest.

ACKNOWLEDGMENTS

The authors acknowledge funding from the U.S. Department of Energy, Office of Basic Energy Sciences, Division of Chemical Sciences, Geosciences, and Biosciences, Separation Science Program, through the Ames National Laboratory. The Ames National Laboratory is operated for the U.S. Department of Energy by Iowa State University of Science and Technology under contract no. DE-AC02-07CH11358. The computational calculations were performed with a grant of computer time at the National Energy Research Scientific Computing Centre (NERSC). NERSC is a DOE Office of Science User Facility supported by the Office of Science of the U.S. DOE under Contract No. DE-AC02-05CH11231. The Materials Analysis Research Laboratory at Iowa State University is acknowledged for providing assistance on SEM-EDS imaging and XPS analysis.

REFERENCES

(1) Kennedy, J. L.; Djeu, N. Operation of Yb: YAG Fiber-Optic Temperature Sensor up to 1600 C. *Sens. Actuators A. Phys.* **2002**, *100* (2−3), 187−191.

(2) Krupke, W. F. Ytterbium Solid-State Lasers. The First Decade. *IEEE J. Sel. Top. Quantum Electron.* **2000**, *6* (6), 1287−1296.

(3) Liu, J.-L.; Yuan, K.; Leng, J.-D.; Ungur, L.; Wernsdorfer, W.; Guo, F.-S.; Chibotaru, L. F.; Tong, M.-L. A Six-Coordinate Ytterbium

Complex Exhibiting Easy-Plane Anisotropy and Field-Induced Single-Ion Magnet Behavior. *Inorg. Chem.* **2012**, *51* (15), 8538−8544.
(4) Patel, N. S.; Fan, P.; Chiu-Tsao, S.-T.; Ravi, K.; Sherman, W.; Quon, H.; Pisch, J.; Tsao, H.-S.; Harrison, L. B. Ytterbium-169: A Promising New Radionuclide for Intravascular Brachytherapy. *Cardiovasc. Radiat. Med.* **2001**, *2* (3), 173−180.
(5) Liu, Y.; Ai, K.; Liu, J.; Yuan, Q.; He, Y.; Lu, L. A High-performance Ytterbium-based Nanoparticulate Contrast Agent for in Vivo X-ray Computed Tomography Imaging. *Angew. Chem.* **2012**, *124* (6), 1466−1471.
(6) Khan, A. M.; Yusoff, I.; Bakar, N. K. A.; Bakar, A. F. A.; Alias, Y. Assessing Anthropogenic Levels, Speciation, and Potential Mobility of Rare Earth Elements (REEs) in Ex-Tin Mining Area. *Environ. Sci. Pollut. Res.* **2016**, *23*, 25039−25055.
(7) Ambaye, T. G.; Vaccari, M.; Castro, F. D.; Prasad, S.; Rtimi, S. Emerging Technologies for the Recovery of Rare Earth Elements (REEs) from the End-of-Life Electronic Wastes: A Review on Progress, Challenges, and Perspectives. *Environ. Sci. Pollut. Res.* **2020**, *27*, 36052−36074.
(8) Han, K. N. Characteristics of Precipitation of Rare Earth Elements with Various Precipitants. *Minerals* **2020**, *10* (2), 178.
(9) Chi, R.; Xu, Z. A Solution Chemistry Approach to the Study of Rare Earth Element Precipitation by Oxalic Acid. *Metall. Mater. Trans. B* **1999**, *30*, 189−195.
(10) Manchanda, V. K.; Chang, C. A. Solvent Extraction Studies of Europium (III), Ytterbium (III), and Lutetium (III) with Ionizable Macrocyclic Ligands and Thenoyltrifluoroacetone. *Anal. Chem.* **1987**, *59* (6), 813−818.
(11) Ochsenkühn-Petropulu, M.; Lyberopulu, T.; Parissakis, G. Selective Separation and Determination of Scandium from Yttrium and Lanthanides in Red Mud by a Combined Ion Exchange/Solvent Extraction Method. *Anal. Chim. Acta* **1995**, *315* (1−2), 231−237.
(12) Holbrey, J. D.; Seddon, K. R. Ionic Liquids. *Clean products and processes* **1999**, *1* (4), 223−236.
(13) Patel, R.; Kumari, M.; Khan, A. B. Recent Advances in the Applications of Ionic Liquids in Protein Stability and Activity: A Review. *Appl. Biochem. Biotechnol.* **2014**, *172*, 3701−3720.
(14) Earle, M. J.; Seddon, K. R. Ionic Liquids. Green Solvents for the Future. *Pure Appl. Chem.* **2000**, *72* (7), 1391−1398.
(15) Bhat, A. R.; Padder, R. A.; Husain, M.; Patel, R. Development of Cholinium-Based API Ionic Liquids with Enhanced Drug Solubility: Biological Evaluation and Interfacial Properties. *Mol. Pharmaceutics* **2024**, *21* (2), 535−549.
(16) Wang, K.; Adidharma, H.; Radosz, M.; Wan, P.; Xu, X.; Russell, C. K.; Tian, H.; Fan, M.; Yu, J. Recovery of Rare Earth Elements with Ionic Liquids. *Green Chem.* **2017**, *19* (19), 4469−4493.
(17) Sun, X.; Luo, H.; Dai, S. Solvent Extraction of Rare-Earth Ions Based on Functionalized Ionic Liquids. *Talanta* **2012**, *90*, 132−137.
(18) Khodakarami, M.; Alagha, L. Separation and Recovery of Rare Earth Elements Using Novel Ammonium-Based Task-Specific Ionic Liquids with Bidentate and Tridentate O-Donor Functional Groups. *Sep. Purif. Technol.* **2020**, *232*, No. 115952.
(19) Kubota, F.; Shimobori, Y.; Baba, Y.; Koyanagi, Y.; Shimojo, K.; Kamiya, N.; Goto, M. Application of Ionic Liquids to Extraction Separation of Rare Earth Metals with an Effective Diglycol Amic Acid Extractant. *J. Chem. Eng. Jpn.* **2011**, *44* (5), 307−312.
(20) Tazoe, H.; Obata, H.; Yamagata, T.; Karube, Z.; Nagai, H.; Yamada, M. Determination of Strontium-90 from Direct Separation of Yttrium-90 by Solid Phase Extraction Using DGA Resin for Seawater Monitoring. *Talanta* **2016**, *152*, 219−227.
(21) Chen, Z.; Yang, X.; Song, L.; Wang, X.; Xiao, Q.; Xu, H.; Feng, Q.; Ding, S. Extraction and Complexation of Trivalent Rare Earth Elements with Tetraalkyl Diglycolamides. *Inorg. Chim. Acta* **2020**, *513*, No. 119928.
(22) Yang, F.; Kubota, F.; Baba, Y.; Kamiya, N.; Goto, M. Selective Extraction and Recovery of Rare Earth Metals from Phosphor Powders in Waste Fluorescent Lamps Using an Ionic Liquid System. *J. Hazard Mater.* **2013**, *254*−*255* (1), 79−88.
(23) Chen, Q.; Lu, C.; Hu, Y.; Liu, Y.; Zhou, Y.; Jiao, C.; Zhang, M.; Hou, H.; Gao, Y.; Tian, G. Extraction Behavior of Several Lanthanides from Nitric Acid with DMDODGA in [C4mim][NTf2] Ionic Liquid. *J. Radioanal. Nucl. Chem.* **2021**, *327* (1), 565−573.
(24) Freire, M. G.; Neves, C. M. S. S.; Marrucho, I. M.; Coutinho, J. A. P.; Fernandes, A. M. Hydrolysis of Tetrafluoroborate and Hexafluorophosphate Counter Ions in Imidazolium-Based Ionic Liquids. *J. Phys. Chem. A* **2010**, *114* (11), 3744−3749.
(25) Rout, A.; Kotlarska, J.; Dehaen, W.; Binnemans, K. Liquid−Liquid Extraction of Neodymium (III) by Dialkylphosphate Ionic Liquids from Acidic Medium: The Importance of the Ionic Liquid Cation. *Phys. Chem. Chem. Phys.* **2013**, *15* (39), 16533−16541.
(26) Rout, A.; Venkatesan, K. A.; Srinivasan, T. G.; Vasudeva Rao, P. R. Extraction and Third Phase Formation Behavior of Eu(III) IN CMPO−TBP Extractants Present in Room Temperature Ionic Liquid. *Sep. Purif. Technol.* **2011**, *76* (3), 238−243.
(27) Zhou, H.; Wang, Y.; Guo, X.; Dong, Y.; Su, X.; Sun, X. The Recovery of Rare Earth by a Novel Extraction and Precipitation Strategy Using Functional Ionic Liquids. *J. Mol. Liq.* **2018**, *254*, 414−420.
(28) Edoardo, A.; Bylaska, E.; de Jong, W.; Govind, N.; Kowalski, K.; Straatsma, T. P.; Valiev, M.; van Dam, H. J. J.; Alexeev, Y.; Anchell, J. NWChem: Past, Present, and Future. *J. Chem. Phys.* **2020**, *152* (18), No. 182102.
(29) Lee, C.; Yang, W.; Parr, R. G. Development of the Colle-Salvetti Correlation-Energy Formula into a Functional of the Electron Density. *Phys. Rev. B* **1988**, *37* (2), 785.
(30) Becke, A. D. Density-functional Thermochemistry. I. The Effect of the Exchange-only Gradient Correction. *J. Chem. Phys.* **1992**, *96* (3), 2155−2160.
(31) Weigend, F.; Ahlrichs, R. Balanced Basis Sets of Split Valence, Triple Zeta Valence and Quadruple Zeta Valence Quality for H to Rn: Design and Assessment of Accuracy. *Phys. Chem. Chem. Phys.* **2005**, *7* (18), 3297−3305.
(32) Weigend, F. Accurate Coulomb-Fitting Basis Sets for H to Rn. *Phys. Chem. Chem. Phys.* **2006**, *8* (9), 1057−1065.
(33) Schuchardt, K. L.; Didier, B. T.; Elsethagen, T.; Sun, L.; Gurumoorthi, V.; Chase, J.; Li, J.; Windus, T. L. Basis Set Exchange: A Community Database for Computational Sciences. *J. Chem. Inf. Model* **2007**, *47* (3), 1045−1052.
(34) Pritchard, B. P.; Altarawy, D.; Didier, B.; Gibson, T. D.; Windus, T. L. New Basis Set Exchange: An Open, up-to-Date Resource for the Molecular Sciences Community. *J. Chem. Inf. Model* **2019**, *59* (11), 4814−4820.
(35) Grimme, S.; Antony, J.; Ehrlich, S.; Krieg, H. A Consistent and Accurate Ab Initio Parametrization of Density Functional Dispersion Correction (DFT-D) for the 94 Elements H-Pu. *J. Chem. Phys.* **2010**, *132* (15), No. 154104.
(36) Marenich, A. V.; Cramer, C. J.; Truhlar, D. G. Universal Solvation Model Based on Solute Electron Density and on a Continuum Model of the Solvent Defined by the Bulk Dielectric Constant and Atomic Surface Tensions. *J. Phys. Chem. B* **2009**, *113* (18), 6378−6396.
(37) Anderson, J. L.; Ding, J.; Welton, T.; Armstrong, D. W. Characterizing Ionic Liquids on the Basis of Multiple Solvation Interactions. *J. Am. Chem. Soc.* **2002**, *124* (47), 14247−14254.
(38) Wakai, C.; Oleinikova, A.; Ott, M.; Weingärtner, H. How Polar Are Ionic Liquids? Determination of the Static Dielectric Constant of an Imidazolium-Based Ionic Liquid by Microwave Dielectric Spectroscopy. *J. Phys. Chem. B* **2005**, *109* (36), 17028−17030.
(39) Nikolaienko, T. Y.; Bulavin, L. A. Localized Orbitals for Optimal Decomposition of Molecular Properties. *Int. J. Quantum Chem.* **2019**, *119* (3), No. e25798.
(40) Nikolaienko, T. Y.; Bulavin, L. A.; Hovorun, D. M. JANPA: An Open Source Cross-Platform Implementation of the Natural Population Analysis on the Java Platform. *Comput. Theor. Chem.* **2014**, *1050*, 15−22.

https://doi.org/10.1021/acsomega.4c06091
ACS Omega 2024, 9, 40134−40144

(41) Shimojo, K.; Nakai, A.; Okamura, H.; Saito, T.; Ohashi, A.; Naganawa, H. Comprehensive Extraction Study Using N. *N*-Dioctyldiglycolamic Acid. *Anal. Sci.* **2014**, *30* (4), 513−517.
(42) Yang, F.; Baba, Y.; Kubota, F.; Kamiya, N.; Goto, M. Extraction and Separation of Rare Earth Metal Ions with DODGAA in Ionic Liquids. *Solvent Extr. Res. Dev. Japan* **2012**, *19*, 69−76.
(43) Usma, C. L.; Dourdain, S.; Arrachart, G.; Pellet-Rostaing, S. Solvent Extraction of Rare Earths Elements from Nitrate Media in DMDOHEMA/Ionic Liquid Systems: Performance and Mechanism Studies. *RSC Adv.* **2021**, *11* (50), 31197−31207.
(44) Billard, I.; Ouadi, A.; Gaillard, C. Liquid−Liquid Extraction of Actinides, Lanthanides, and Fission Products by Use of Ionic Liquids: From Discovery to Understanding. *Anal. Bioanal. Chem.* **2011**, *400* (6), 1555−1566.
(45) Maria, L.; Cruz, A.; Carretas, J. M.; Monteiro, B.; Galinha, C.; Gomes, S. S.; Araújo, M. F.; Paiva, I.; Marcalo, J.; Leal, J. P. Improving the Selective Extraction of Lanthanides by Using Functionalised Ionic Liquids. *Sep. Purif. Technol.* **2020**, *237*, No. 116354.
(46) Sasaki, Y.; Rapold, P.; Arisaka, M.; Hirata, M.; Kimura, T.; Hill, C.; Cote, G. An Additional Insight into the Correlation between the Distribution Ratios and the Aqueous Acidity of the TODGA System. *Solvent Extr. Ion Exch.* **2007**, *25* (2), 187−204.
(47) Ravi, J.; Venkatesan, K. A.; Antony, M. P.; Srinivasan, T. G.; Vasudeva Rao, P. R. Tuning the Diglycolamides for Modifier-Free Minor Actinide Partitioning. *J. Radioanal. Nucl. Chem.* **2013**, *295* (2), 1283−1292.
(48) Ma, F.; Du, C.; Zheng, S.; Du, Y. In Situ Monitoring of Nitrate Content in Leafy Vegetables Using Attenuated Total Reflectance−Fourier-Transform Mid-Infrared Spectroscopy Coupled with Machine Learning Algorithm. *Food Anal. Methods* **2021**, *14* (11), 2237−2248.
(49) Xu, H.; Wu, C.; Li, H.; Chu, J.; Sun, G.; Xu, Y.; Yan, Y. Synthesis, Characterization and Photocatalytic Activities of Rare Earth-Loaded BiVO4 Catalysts. *Appl. Surf. Sci.* **2009**, *256* (3), 597−602.
(50) Da Cunha, M.; Weber, M.; Nart, F. C. On the Adsorption and Reduction of NO3−Ions at Au and Pt Electrodes Studied by in Situ FTIR Spectroscopy. *J. Electroanal. Chem.* **1996**, *414* (2), 163−170.
(51) Chastain, J.; King, R. C., Jr. *Handbook of X-Ray Photoelectron Spectroscopy*; Perkin-Elmer Corporation, 1992; Vol. *40*, p 221.
(52) Shimojo, K.; Fujiwara, I.; Fujisawa, K.; Okamura, H.; Sugita, T.; Oshima, T.; Baba, Y.; Naganawa, H. Extraction Behavior of Rare-Earth Elements Using a Mono-Alkylated Diglycolamic Acid Extractant. *Solvent Extr. Res. Dev., Jpn.* **2016**, *23* (2), 151−159.
(53) Wagner, C. D.; Naumkin, A. V; Kraut-Vass, A.; Allison, J. W.; Powell, C. J.; Rumble, Jr, J. R. *NIST Standard Reference Database 20, Version 3.4 (Web Version)*; National Institute of Standards and Technology: Gaithersburg, MD, 2003; p 20899.
(54) Hosangadi, B. D.; Dave, R. H. An Efficient General Method for Esterification of Aromatic Carboxylic Acids. *Tetrahedron Lett.* **1996**, *37* (35), 6375−6378.

https://doi.org/10.1021/acsomega.4c06091
ACS Omega 2024, 9, 40134−40144